Faraday Discussions

Cite this: *Faraday Discuss.*, 2016, **194**, 659

PAPER

Towards efficient time-resolved X-ray absorption studies of electron dynamics at photocatalytic interfaces

Stefan Neppl,*[a] Johannes Mahl,[a] Anton S. Tremsin,[b] Bruce Rude,[c] Ruimin Qiao,[c] Wanli Yang,[c] Jinghua Guo[c] and Oliver Gessner*[a]

Received 10th May 2016, Accepted 18th May 2016
DOI: 10.1039/c6fd00125d

We present a picosecond time-resolved X-ray absorption spectroscopy (tr-XAS) setup designed for synchrotron-based studies of interfacial photochemical dynamics. The apparatus combines a high power, variable repetition rate picosecond laser system with a time-resolved X-ray fluorescence yield detection technique. Time-tagging of the detected fluorescence signals enables the parallel acquisition of X-ray absorption spectra at a variety of pump–probe delays employing the well-defined time structure of the X-ray pulse trains. The viability of the setup is demonstrated by resolving dynamic changes in the fine structure near the O1s X-ray absorption edge of cuprous oxide (Cu_2O) after photo-excitation with a 355 nm laser pulse. Two distinct responses are detected. A pronounced, quasi-static, reversible change of the Cu_2O O1s X-ray absorption spectrum by up to ~30% compared to its static line shape corresponds to a redshift of the absorption edge by ~1 eV. This value is small compared to the 2.2 eV band gap of Cu_2O but in agreement with previously published results. The lifetime of this effect exceeds the laser pulse-to-pulse period of 8 μs, resulting in a quasi-static spectral change that persists as long as the sample is exposed to the laser light, and completely vanishes once the laser is blocked. Additionally, a short-lived response corresponding to a laser-induced shift of the main absorption line by ~2 eV to lower energies appears within <200 ps and decays with a characteristic timescale of 43 ± 5 ns. Both the picosecond rise and nanosecond decay of this X-ray response are simultaneously captured by making use of a time-tagging approach – highlighting the prospects of the experimental setup for efficient probing of the electronic and structural dynamics in photocatalytic systems on multiple timescales.

[a]*Chemical Sciences Division, Lawrence Berkeley National Laboratory, Berkeley, California, USA. E-mail: ogessner@lbl.gov; sneppl@lbl.gov*
[b]*Space Sciences Laboratory, University of California, Berkeley, California, USA*
[c]*Advanced Light Source, Lawrence Berkeley National Laboratory, Berkeley, California, USA*

Introduction

At the heart of many emerging sunlight-to-fuel and sunlight-to-electricity concepts are interfacial processes that require an optimized, concerted flow of charge and energy on the molecular level. Microscopic processes evolving on spatial and temporal scales spanning orders of magnitudes have to be connected in order to gain comprehensive insight into the mechanisms that govern the efficiency of macroscopic charge and energy transport. Soft X-ray spectroscopy techniques have the potential to probe electronic and chemical states of matter with atomic site-specificity and chemical sensitivity, which is required to improve our fundamental understanding of interfacial chemistry and photophysics in complex systems. Over the last decade, *in situ* and *in operando* X-ray absorption and X-ray photoemission techniques have been developed at several synchrotron radiation facilities and are now routinely being used to probe the chemical and structural properties of photo-catalytic interfaces including oxidation state changes, local redox activity, elemental composition, as well as the electronic characters of chemically active states under realistic working conditions.[1–8]

While such (quasi-) static experiments are valuable for shedding light on fundamental chemical transformations, they are only sensitive to chemical species and electronic configurations with sufficiently long lifetimes such that their time-averaged concentration is above the detection limit. The identification of short-lived intermediates states, however, which frequently play a decisive role for the overall outcome and efficiency of photochemical reactions, is often impossible. This limitation has been overcome in the optical regime by the development of ultrafast NIR/Vis and UV time-resolved spectroscopy techniques, which nowadays form the experimental backbone of the field of femtochemistry.[9] Despite their remarkable sensitivity and superb time-resolution, however, gaining comprehensive microscopic insight into electronic and nuclear dynamics in large, heterogeneous systems, such as complex interfaces using solely ultrafast all-optical spectroscopy, is extremely challenging: in particular, spectroscopic fingerprints of different system components may overlap due to the delocalized nature of optically driven valence electron transitions, which denies an atomic-scale perspective on the ensuing chemical dynamics.

In contrast, the simultaneous element specificity and chemical sensitivity of X-ray transitions can potentially offer a significantly more distinct probe of local chemical transformations. Consequently, tremendous efforts have been devoted over the past decade to extend the power of ultrafast spectroscopy for real-time probing of chemical dynamics into the X-ray regime. Laboratory,[10–12] synchrotron[13–19] and free-electron laser based[20–25] methods have been explored in order to combine the sensitivity of inner-shell transitions to the local valence electronic structure with the capability of time-domain techniques to reveal transient charge configurations.

Here, we report on the progress toward developing a picosecond time-resolved transient X-ray absorption spectroscopy (tr-XAS) capability for time-domain *in situ* studies of interfacial photochemistry, which is currently being implemented at the Advanced Light Source (ALS). Absorption spectra are recorded in total X-ray fluorescence yield (TFY) mode, *i.e.*, in a photon-in/photon-out configuration rather than in transmission geometry, in order to be compatible with a wide

variety of materials and existing *in situ*/*operando* soft X-ray spectroscopy techniques.[1,2,26] The setup is based on the combination of a high repetition rate picosecond laser system with a microchannel plate (MCP) based time- and position-sensitive delay-line detector.[27] The detector is used to simultaneously record and discriminate the TFY signals induced by individual X-ray pulses of the ALS bunch train by adopting a time-tagging data acquisition approach.[28] The mobile system can be deployed at various beamlines and is compatible with all synchrotron operating modes and electron bunch filling patterns.

The viability of the picosecond tr-XAS apparatus is demonstrated by monitoring photo-induced dynamics in the near-edge X-ray absorption fine structure of cuprous oxide (Cu_2O) in the vicinity of the O1s absorption edge. This metal oxide semiconductor is a promising electrode material for a number of photochemical applications, *e.g.* photocatalytic water splitting, where a detailed understanding of the photo-induced charge carrier dynamics in the bulk and at the metal oxide–liquid interface is crucial for the design of successful device architectures.[29–31]

In the experiment presented here, a Cu_2O powder sample is excited with 10 ps, 355 nm (3.5 eV) pulses, *i.e.*, significantly above the ~2.2 eV optical band gap,[32–34] using laser pulse fluences of ~6–10 mJ cm^{-2}. A pronounced, reversible spectral change of the O1s XAS line shape is observed upon laser illumination that remains constant as long as the sample is exposed to laser light and completely vanishes when the laser is turned off. Considering the laser repetition rate of 127 kHz, the lifetime of this effect must be much longer than 8 μs. The quasi-static spectral response may be described by an effective shift of a Gaussian shaped near-edge spectral component to ~1 eV lower photon energies. The magnitude of this shift is in agreement with the findings by Gaffney and co-workers, who probed the dynamics in a thin polycrystalline film of Cu_2O by tr-XAS in transmission mode at a similar laser excitation fluence.[35]

In addition to this quasi-static response, a short-lived laser-induced modification of the O1s XAS spectrum develops within a rise time of less than 200 ps after photo-excitation and may be described by an effective spectral shift of ~2 eV to lower photon energies. The temporal evolution of this transient XAS response follows a mono-exponential decay with a characteristic time constant of 43 ± 5 ns. Notably, the spectral shift associated with this short-lived response is comparable to the band gap energy of Cu_2O (2.2 eV), while the quasi-static response manifests itself in a significantly smaller shift.[32–34] The results are discussed in the light of previous static and time-resolved XAS experiments on Cu_2O and with respect to possible electronic and structural dynamics that may underlie the photo-induced changes in the O1s XAS spectrum.

Experimental details

The feasibility of picosecond tr-XAS has been demonstrated at several synchrotron radiation facilities,[14,28,36–38] with the main focus of research being the investigation of photochemical dynamics in liquid jets.[13,14,16] A temporal resolution limited only by the length of the electron bunches inside the storage ring (30–100 ps) can be routinely achieved. The efficiency of these experiments has recently been significantly improved by using high-power, high-repetition rate picosecond lasers as excitation sources instead of femtosecond kHz Ti:sapphire systems.[37,38]

In the commonly adapted pump–probe tr-XAS approach, gated detectors (typically avalanche photodiodes) are used to record the X-ray fluorescence or transmission signal related to a single X-ray pulse at one specific pump–probe delay at a time. Evidently, such techniques can only use a tiny fraction of the MHz X-ray pulse trains available at third-generation synchrotrons to probe the laser-induced dynamics in the target, which results in a significantly reduced data collection efficiency compared to static X-ray measurements. Recently, Stebel *et al.* demonstrated that replacing the gated (slow) diode with a fast time-resolving detector enables laser-pump/multiple X-ray probe data acquisition schemes that can efficiently sample transient changes in XAS spectra over hundreds of nanoseconds simultaneously.[28]

Fig. 1 illustrates the tr-XAS setup implemented at the Advanced Light Source (ALS). It combines a flexible picosecond laser system[37–39] with a fast MCP/delay line detector[27] with the goal to enable studies of photochemical reactions in a wide range of solids and solid–molecular interfaces on pico- to nanosecond

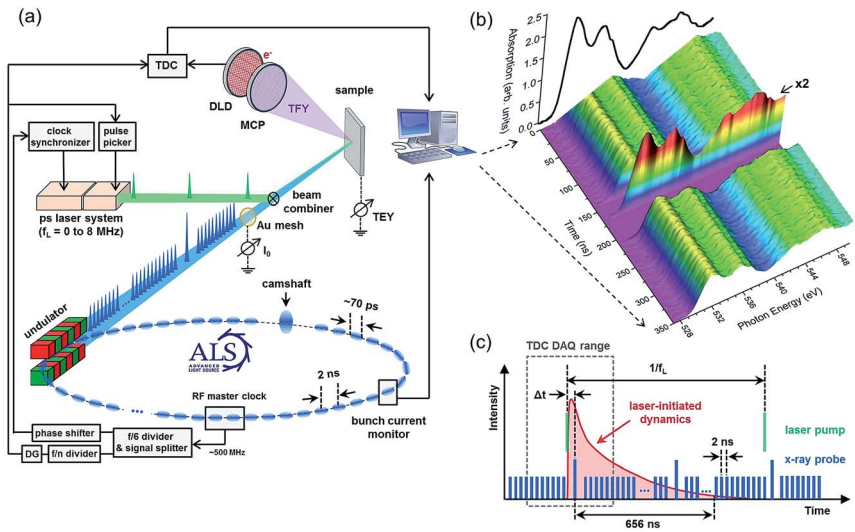

Fig. 1 Overview of the picosecond time-resolved X-ray absorption (tr-XAS) setup currently operated at the Advanced Light Source (ALS). (a) Schematic view of key components of the experiment including the electronic timing scheme applied to achieve and control the synchronisation between the laser pulses and the ALS X-ray pulse train. See text for details. (b) Example of time- and photon-energy-dependent total X-ray fluorescence yield (TFY) spectra obtained from a TiO_2 nanoparticle film at the O1s edge. The fast time-resolved detector and associated electronics enable the unambiguous assignment of TFY signals to individual X-ray pulses within the 500 MHz X-ray pulse train. Note that the apparent merging of the multi-bunch signals is the result of the image rendering routine. A more detailed view of the individual bunch signals is presented in Fig. 2. All tr-XAS traces are individually normalized to the X-ray pulse fluence based on the corresponding electron bunch charges measured inside the storage ring. The data is further corrected for the photon-energy-dependent X-ray transmission of the beamline by using the photocurrent of a gold mesh inserted into the X-ray beam as a reference. The time-averaged total electron yield (TEY) spectrum of the sample (black solid line) is recorded simultaneously with the time-resolved TFY data. (c) Principle of laser-pump/multiple X-ray probe spectroscopy during ALS multi-bunch operating mode.

timescales. Both the laser system and the high-vacuum endstation (base pressure $<5 \times 10^{-9}$ mbar) that accommodates the detector, beam steering optics and diagnostic tools, as well as the motorized sample manipulator, are mobile, flexible units, enabling tr-XAS experiments at a variety of ALS beamlines.

The measurements presented here have been performed at the soft X-ray undulator beamline 8.0.1. The sample is excited with 355 nm laser pulses at a repetition rate of 127 kHz. The corresponding photon energy of 3.5 eV enables efficient generation of electron–hole pairs by excitation above the ~2.2 eV direct band gap of Cu_2O.[32–34] The ensuing charge dynamics due to, *e.g.* carrier trapping and recombination, are probed by monitoring transient spectral changes near the O1s X-ray absorption edge. Since both the valence band (VB) and the bottom of the conduction band (CB) in Cu_2O are derived predominantly from O2p and Cu3d states,[40–42] the dipole allowed O1s → O2p X-ray transitions provide – in principle – simultaneous sensitivity to the generation of VB vacancies and the population of the CB states upon laser excitation.

Laser-X-ray synchronization

A critical issue in synchrotron-based laser-pump/X-ray probe experiments is the precise and long-term stable synchronization of the two independent light sources. The electronic layout to control the phase relation between the laser and the X-ray pulse train in the tr-XAS experiment presented here is shown Fig. 1(a). It is based on a previously described synchronisation scheme that has been successfully applied in time-resolved X-ray photoemission experiments at the ALS.[39,43] Briefly, the ~500 MHz master clock signal of the ALS storage ring is down-converted to ~83 MHz and split into two signal branches. A clock synchronizer is used to phase-lock the laser oscillator with a typical jitter of <1 ps (rms) to the reference signal supplied by the first branch. The frequency of the second signal output can be further adjusted and delayed using a programmable frequency divider and an electronic delay generator (DG). This signal is used to trigger both the pulse picker inside the laser amplifier, and to start the data acquisitions of the time-to-digital converter (TDC) that counts all photons registered by the detector and determines their arrival time with respect to the start signal within a time window of ~350 ns. The time delay between the laser pulses and the X-ray pulse train can be adjusted in steps of the 12 ns oscillator roundtrip time using the DG in the pulse picker synchronization branch. Additionally, time delays with a minimum step size of 5 ps can be set electronically using a phase shifter unit with a total delay range 5 ns in the oscillator feedback loop. This robust and flexible timing scheme has proven to provide reliable synchronisation between the X-ray and laser pulse with sub-picosecond accuracy for several days.[43]

The employed laser system is a commercial high-power picosecond laser (DUETTO™, Time-Bandwidth Products) delivering 10 ps pulses at user-selectable repetition rates between the single-shot limit and 8 MHz. In addition to the fundamental wavelength of 1064 nm, internal frequency doubling and tripling stages provide 532 nm and 355 nm laser pulses.

Data acquisition and normalisation scheme

Typical time-resolved total fluorescence yield XAS data obtained at the O1s edge of a TiO_2 test sample is shown in Fig. 1(b). A cut along the detection time axis at

a fixed photon energy yields a time histogram as shown in Fig. 2(a and b). Evidently, the time-response of the detector is sufficiently fast to resolve all the characteristic features imprinted on the TFY by the standard ALS electron bunch filling pattern, *i.e.*, the 2 ns spaced multi-bunch pulses and the more intense "camshaft" pulse that resides within a 60 ns wide gap between the remaining bunches. Compared to conventional pump–probe methods that record data at one specific pump–probe delay at a time, the time-tagging technique enabled by the fast detector/electronics eliminates the need to explore extended delay ranges with a large number of separate measurements. Instead, the long-term dynamics are automatically sampled within the TDC time window (Fig. 1(c)).

In order to gain accurate spectral information, the measured fluorescence yields have to be normalized with respect to the X-ray flux incident on the sample at each photon energy. For static XAS spectra, it is sufficient to determine the time/bunch-averaged incident X-ray flux by measuring, for example, the photo-current from a gold mesh inserted into the X-ray beam. This procedure is mainly

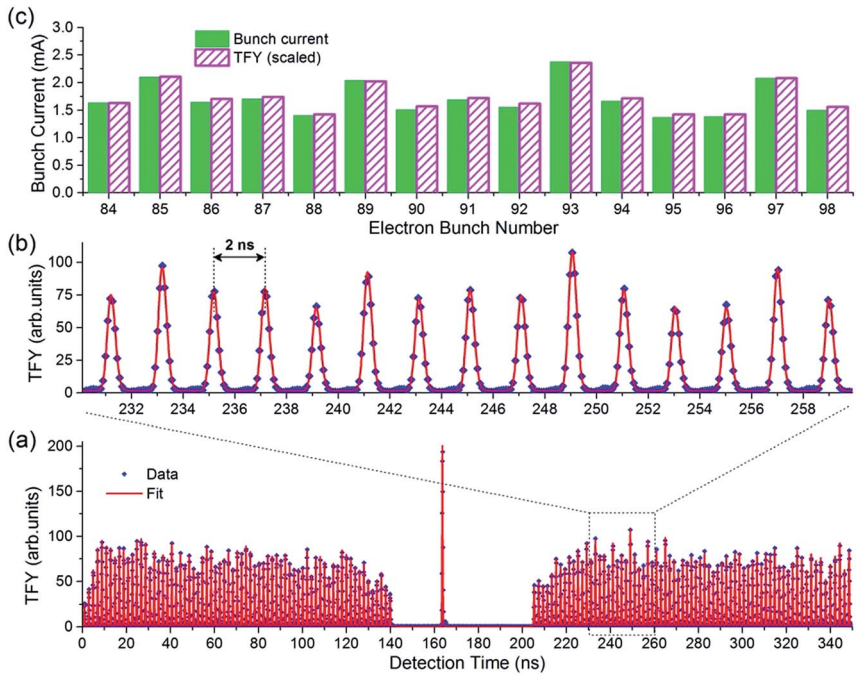

Fig. 2 Correlation between individual bunch currents and TFY signals. (a) Time-resolved TFY (blue markers) from a Cu_2O sample at a fixed photon energy of 532 eV accumulated over 2 min (typical data acquisition time per energy step for high-quality tr-XAS spectra). A global fit of the time histogram to a series of Gaussians with identical FWHMs (red solid line) is used to quantify the TFY intensities (peak areas) induced by the individual X-ray pulses. (b) Enlarged section of the data shown in (a). The overall time resolution of the employed detector/electronics enables an unambiguous separation of the TFY originating from the camshaft pulse and from the 2 ns spaced X-ray pulses within the multi-bunch section of the ALS electron filling pattern. (c) Comparison of the time-resolved TFY to the respective electron bunch currents measured inside the storage ring. A single, global scaling factor has been applied to the TFY intensities to match the TFY of bunch #84 with its bunch current value.

used to correct for the photon-energy dependent transmission of the beamline. In contrast, the tr-XAS traces induced by individual X-ray pulses have to be separately normalized with respect to the X-ray flux associated with specific X-ray pulses. For the data presented here, this bunch-specific flux is estimated by an electron-bunch charge measurement inside the ALS storage ring, which is recorded simultaneously with the time-resolved TFY data.

As illustrated in Fig. 2(c), the bunch charge and the corresponding TFY may vary significantly from bunch to bunch. Moreover, both quantities vary as a function of time due to scattering-induced electron beam losses and frequent bunch refilling events during ALS top-off operating mode. Fig. 3(a) compares the bunch current associated with a specific bunch (#23, red) to the average current of a series of bunches (#1–72, blue) while scanning the photon energy across the O1s

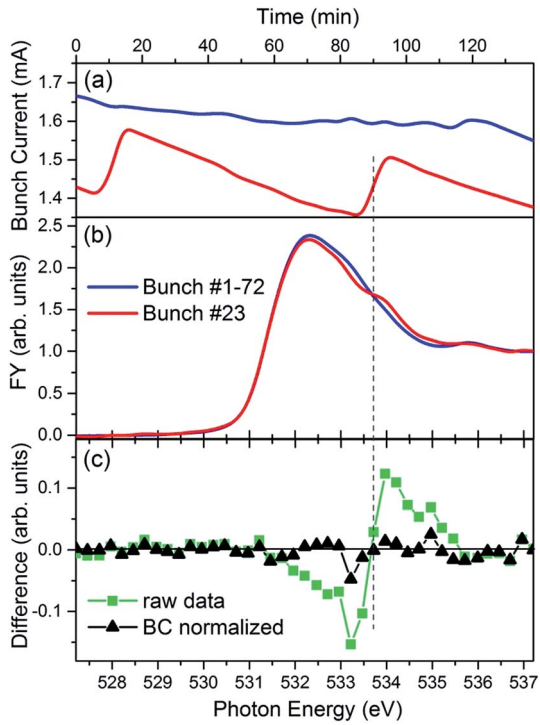

Fig. 3 Importance of individual bunch charge normalization in the tr-XAS experiments. All data were recorded during a single photon energy scan across the entire range starting from the lowest value. Therefore, the photon energy axis represents a time axis with a 2 min point-to-point spacing. (a) The time dependence of individual electron bunch currents inside the ALS storage ring is exemplified by the current of bunch #23 (red solid line). The spurious effects of the characteristic slow decay and step-like increase of the bunch current due to electron scattering losses and electron bunch refilling events, respectively, are clearly visible. They cannot be completely eliminated by averaging the signal of a large number of bunches, *e.g.* bunches #1–72 (blue solid line). (b) Raw O1s tr-XAS spectra of Cu_2O (without any laser excitation) recorded with the indicated X-ray pulses over the same time span as in (a). A significant distortion of the XAS line shape, mainly because of the refilling of bunch #23 during the photon energy scan, is evident. (c) Difference of the two XAS spectra before (green squares) and after (black triangles) normalization to the individual bunch current values shown in (a).

edge region of a Cu_2O sample. In contrast to the relatively stable average current, the individual bunch current undergoes large (~10%) amplitude variations during the time required to record a high-quality XAS spectrum. The importance of an individual bunch charge calibration is highlighted in Fig. 3(b and c). Fig. 3(b) compares the O1s tr-XAS spectra of Cu_2O associated with the same specific bunch (#23, red) and with the series of bunches (#1–72, blue) as used in Fig. 3(a). No laser was employed in this measurement so all X-ray bunches should produce the same spectrum. However, as can be seen in Fig. 3(b), the variations in bunch current and, in particular, the abrupt increase of the bunch charge during refilling leads to significant distortions of the tr-XAS spectral line shape. These intensity variations translate into corresponding amplitude modulations on a similar order of magnitude in the tr-XAS difference spectra. This effect is illustrated by the green curve in Fig. 3(c), which shows the difference between the red and the blue curves in Fig. 3(b). Without further normalization, the significant structures in the difference spectrum would be superimposed on any effect of interest induced by an exciting laser pulse. However, applying the individual bunch normalization scheme reduces these types of systematic artifacts to typically less than 1% as illustrated by the black trace in Fig. 3(c). The remaining variations are mainly defined by the accuracy of the bunch charge measurement. For future experiments, an intrinsic bunch charge normalization scheme is envisioned, whereby the TFY signal from each individual bunch is sampled twice per laser shot, once before the laser pulse arrives at the sample and once thereafter. This procedure will enable the most direct determination of TFY signal variations associated with varying individual bunch currents.

In addition to the time-resolved TFY, the more surface sensitive total electron yield signal (TEY) is measured with a picoammeter collecting the time-averaged X-ray induced photocurrent of the sample.

Beam characterisation and spatiotemporal overlap

It is crucial for tr-XAS experiments to achieve and maintain excellent spatiotemporal overlap between the X-ray and laser beams at the location of the sample for extended periods of time. In particular, for applications where the beams are raster-scanned across the sample during measurements to mitigate the impact of radiation damage, a near-collinear arrangement of the laser-pump and X-ray probe beams is preferred in order to avoid degradation of the spatial overlap as the sample position may change slightly along the beam propagation direction due to mechanical and/or alignment imperfections. The geometric arrangement of the light beams, sample, and detector in the tr-XAS apparatus discussed here is illustrated in Fig. 4(a): a drilled-through laser mirror is positioned (in vacuum) at a 45° angle with respect to the X-rays, which pass through the *ca. Ø* 1 mm central hole of the mirror and hit the sample under normal incidence geometry. The laser beam is collinearly combined with the X-rays by reflecting it off the mirror surface, which forms the upper part of a periscope. The TFY is measured in grazing emission geometry, in order to minimize saturation/self-absorption effects in the XAS spectra.[44] The MCP detector may be optionally covered by a 500 nm thick Al or Ti filter to eliminate background signals due to stray laser light. Fine adjustment of the laser pointing and spot size at the sample position is accomplished with a combination of a picomotor-controlled steering mirror and

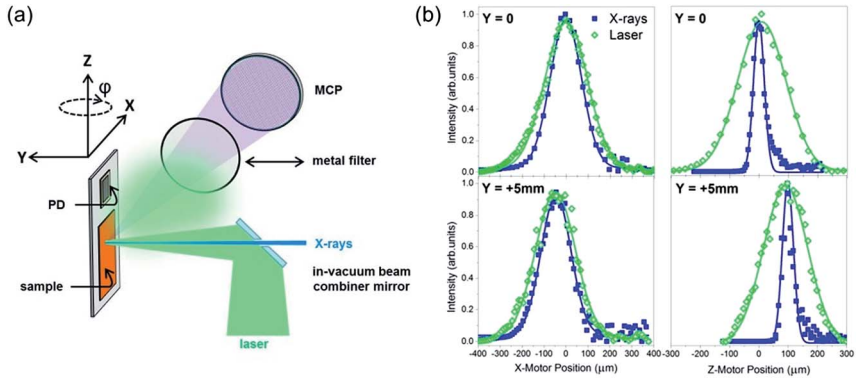

Fig. 4 Details of the pump–probe tr-XAS measurement geometry. (a) Schematic view of the laser and X-ray beam paths, and the arrangement of the sample holder and detector. A drilled-through 45° mirror acts as a beam-combiner that enables a collinear laser/X-ray beam geometry. A 500 nm thick aluminium or titanium metal filter can be translated in front of the detector to block laser stray light. The detector is mounted at a grazing fluorescence detection geometry to minimize saturation/self-absorption effects. (b) Knife-edge scans of the X-ray (blue) and laser (green) beams at different Y positions (along the beam propagation direction) of the sample manipulator. Left and right columns correspond to scans along the horizontal and vertical dimension, respectively. Upper and lower rows correspond to different sample positions along the beam propagation direction. The relative positions of the two beams remain unaffected by moving the sample along the beam propagation direction, demonstrating the robustness of the spatial overlap achieved with the in-vacuum collinear beam-combiner. Minor changes in the absolute beam positions are the result of a small misalignment of the *Y*-axis of the sample manipulator with respect to the beam propagation direction.

a focusing lens mounted on a translation stage outside the vacuum chamber. The sample holder is mounted on a fully motorized, computer-controlled XYZ manipulator, with a total surface area of 5×30 cm^2 available for raster scanning. The large scan area will enable future experiments, *e.g.*, on radiation-sensitive semiconductor–molecule interfaces.[43]

The spatial profiles of the laser and the X-ray beams at the sample position are obtained by performing knife-edge scans with a photodiode mounted directly on the sample holder. Typical results are shown in Fig. 4(b) with the X-ray and laser beam profiles marked by blue and green traces, respectively. The left and right columns of Fig. 4(b) correspond to scans along the horizontal and vertical directions, respectively. A significant astigmatism in the X-ray focus, which is unavoidable at the roll-up port of beamline 8.0.1 of the ALS, is readily apparent. The upper and lower rows of Fig. 4(b) correspond to two sample positions that are 5 mm apart along the beam propagation direction. As a result of the collinear beam geometry, the spatial overlap between the two beams is virtually unaffected by this shift.

The relative timing between the laser pulses and the ALS X-ray pulse train can be adjusted with an accuracy of ± 50 ps by monitoring the response of a fast metal–semiconductor–metal photodiode (rise/fall time < 30 ps) to both beams on a GHz bandwidth oscilloscope. Fine-tuning of the zero pump–probe delay is achieved by using the photoresponse of a suitable sample while scanning the

phase shifter that defines the synchronization of the laser oscillator with the X-ray bunch structure.

Sample characterisation

The cuprous oxide (Cu_2O) sample used in the tr-XAS study presented here consists of Cu_2O powder (566282 Sigma-Aldrich, ≥99.99% trace metal basis) pressed into a *ca.* 2 mm thick Ø 10 mm pellet. No additional sample cleaning is performed after transfer from ambient into vacuum. Static XAS spectra are acquired in order to verify the purity of the sample. The green traces in Fig. 5(a) and (b) show the measured static O1s and Cu2p XAS spectra, respectively, recorded in TEY (solid) and TFY (dashed) modes. The absolute photon energy scale is calibrated by setting the t_{2g} transition energy in the O1s XAS spectrum of a rutile TiO_2 single crystal reference to $h\nu = 530.7$ eV.[45] Except for an overall spectral broadening, the shape of the XAS spectra recorded in TEY and TFY modes agree well with each other, suggesting a very similar chemical composition near the surface and in the bulk of the sample. The broadening in the TFY spectra is likely the result of slightly more pronounced saturation/self-absorption effects compared to the TEY measurements in spite of the grazing detection geometry shown in Fig. 4.[44]

A comparison of the measured spectra with XAS reference data from single crystalline Cu_2O (blue) and CuO (red)[40] confirms the chemical integrity of the Cu_2O powder sample. The main pre-edge features in the O1s and Cu2p XAS spectra of the powder sample at $h\nu = 532.6$ eV and $h\nu = 933.8$ eV, respectively, are

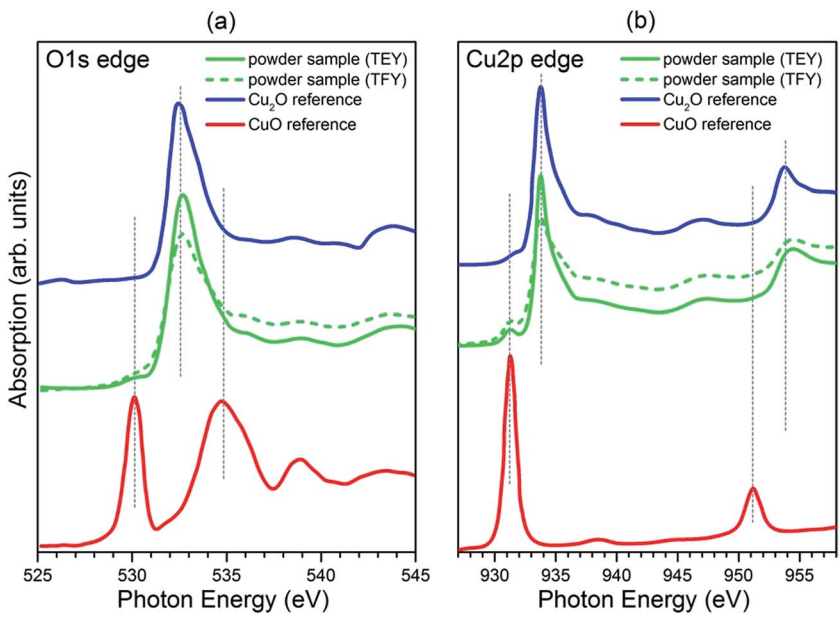

Fig. 5 Characterization of the Cu_2O powder sample. Static O1s (a) and Cu2p (b) XAS spectra recorded in TEY (green solid line) and TFY (green dashed line) are compared to the corresponding reference TEY spectra of single crystalline Cu_2O (blue line) and CuO (red line).[40] Dashed vertical lines indicate transition energies of the most intense absorption features in the reference spectra.

perfectly aligned with the corresponding XAS peaks of the Cu_2O reference. These transitions are due to the excitation of O1s and $Cu2p_{3/2}$ electrons into empty conduction band states with strongly hybridized O2p/Cu3d character.[40,41] The corresponding transitions in CuO occur at *ca.* 2.5 eV lower photon energies. Indeed, a closer inspection of the XAS data in Fig. 5 reveals a small (<5%) but detectable spectral contribution of these transitions to the Cu_2O powder XAS traces.

Results and analysis

For the tr-XAS experiments discussed in the following, the X-ray/laser timing was adjusted such that the laser pulse arrives at the sample $\Delta t = 250$ ps before the camshaft X-ray pulse (Fig. 1(c)). The start trigger for the TDC is adjusted to centre the camshaft signal in the *ca.* 350 ns wide time-recording window of the TDC (Fig. 2(a)). In this way, the tr-XAS traces induced by the ~70 X-ray multi-bunch pulses preceding the laser can be averaged to obtain a high signal-to-noise "pre-laser" ground-state reference, while the X-ray pulses following the camshaft pulse monitor the dynamic evolution of the photo-induced X-ray response at pump–probe delays up to ~180 ns within the same measurement. The laser fluence is varied between 6 mJ cm^{-2} and 10 mJ cm^{-2}, the laser pulse repetition rate is 127 kHz.

The most notable response of the sample to laser excitation is a pronounced, quasi-static broadening and redshift of the main absorption feature near $h\nu = 532$ eV compared to the static O1s XAS spectrum as illustrated in Fig. 6(a). As long as the laser is illuminating the sample, the steady-state "laser-on" XAS spectrum is represented by the red curve, rather than the blue "laser-off" curve that has been measured before laser exposure with 10 mJ cm^{-2}. The dashed green laser-off curve has been measured after laser illumination of the sample. The two laser-off curves are almost identical, demonstrating that the dramatic photo-induced spectral changes are entirely reversible. The quasi-static nature of the effect indicates that the 355 nm laser pulse modulates the X-ray response of the Cu_2O sample on a timescale that significantly exceeds the 8 μs pulse-to-pulse spacing of the 127 kHz laser excitation. The excellent agreement between the blue and green traces in Fig. 6(a) verifies that the effect is not related to an irreversible chemical or structural modification of the Cu_2O sample. Moreover, the corresponding TEY spectra exhibit a very similar behaviour (not shown), suggesting that the mechanism provoking this phenomenon involves both the bulk and the surface of the Cu_2O sample.

The blue trace in Fig. 6(b) shows the difference between the laser-on and the laser-off spectra. Positive features indicate laser-induced enhancement of X-ray absorption, negative features indicate reduced absorption. Applying the method proposed by Hillyard *et al.*,[35] the predominant response between ~529 eV and ~535 eV is analysed in terms of an XAS edge shift that is represented by two Gaussian-shaped spectral contributions: a negative Gaussian at higher energies representing suppressed absorption and a positive Gaussian at lower energies representing enhanced absorption. Using a nonlinear least-squares fit procedure, the positions, widths, and intensities of both model peaks are derived from the measured difference curve, leading to an estimated redshift of the absorption edge by ~0.8 eV.

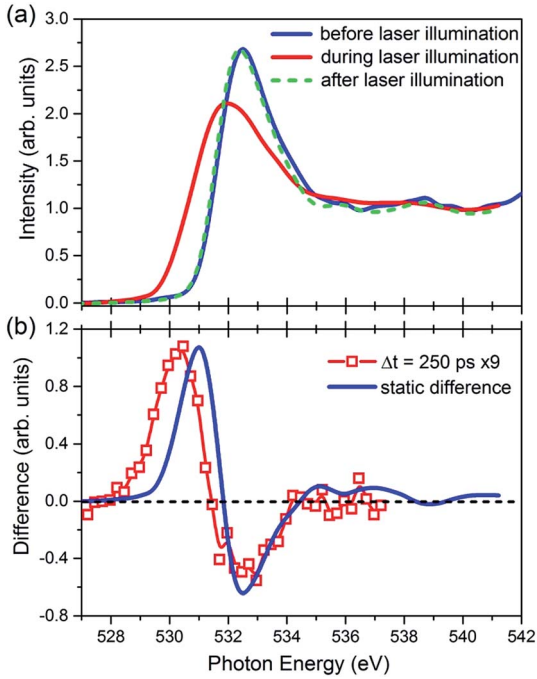

Fig. 6 Evidence for a transient X-ray response with a micro-to-millisecond lifetime. (a) Static O1s XAS spectra recorded before (blue solid line), during (red solid line) and after (green dashed line) illumination of the of Cu_2O sample with the 355 nm laser (10 mJ cm^{-2}; 127 kHz; 0.9 W). (b) The difference of the static laser-on and laser-off XAS spectrum (blue line) is compared to the scaled tr-XAS difference spectrum at $\Delta t = 250$ ps (red squares).

In addition to the quasi-static response, a fast decaying response is observed as illustrated in Fig. 6 and 7. Fig. 7(a) compares the camshaft-related tr-XAS spectrum at $\Delta t = 250$ ps to the pre-laser reference (note that "pre-laser" refers to a spectrum recorded just before the next laser pulse arrives at the sample, which is different from the "laser-off" spectra recorded with the laser output being completely blocked). A distinct laser-induced redshift of the main absorption feature is clearly discernible, which manifests itself in a characteristic bimodal difference spectrum exhibiting a positive and negative amplitude as shown in Fig. 7(b) for a variety of pump–probe delays. The amplitude of the positive peak is a strong function of the pump–probe delay, decaying by more than 70% over a 180 ns time span, whereas the amplitude of the negative peak remains almost constant within the accuracy of the measurement. Moreover, Fig. 7(c) reveals that the spectral shape of the positive peak in the difference spectrum is also affected by the laser fluence, featuring a significant broadening towards lower photon energies when the laser fluence is increased from 6 mJ cm^{-2} to 10 mJ cm^{-2}.

Fig. 8 illustrates the temporal evolution of the positive difference peak amplitude, measured as the peak height ($\Delta t < 500$ ps) or the peak area ($\Delta t > 500$ ps) for different delays. The onset of the response is measured by varying the pump–probe delay (using the phase-shifter unit) between $\Delta t = -500$ and +500 ps. As shown in the inset in Fig. 8, the transient X-ray response is already fully developed within 200 ps. We note that a time resolution of < 100 ps has been demonstrated in time-

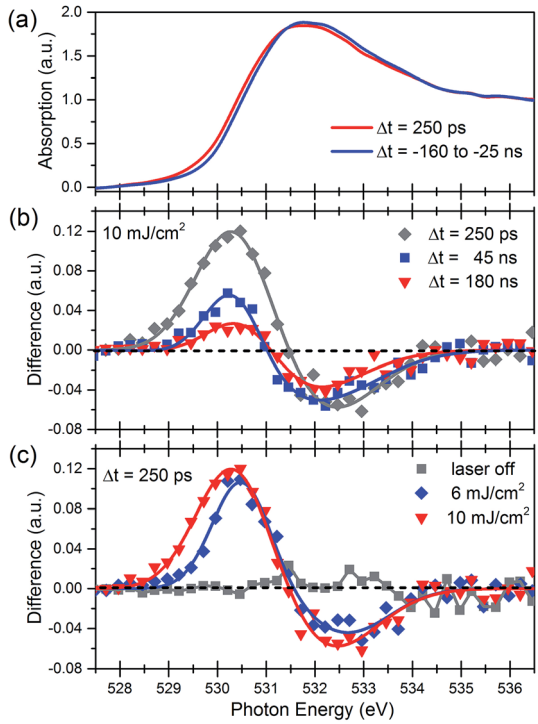

Fig. 7 Laser-induced transient XAS response at the O1s edge of Cu_2O. (a) The tr-XAS spectrum at a pump–probe delay $\Delta t = 250$ ps after 355 nm laser excitation (red solid line) is compared to the tr-XAS spectrum obtained by averaging the XAS signals induced by the 72 X-ray pulses preceding the laser pulse (blue solid line). Post-laser–pre-laser tr-XAS difference spectra recorded with the same laser fluence at different delays Δt, and at a fixed Δt but different laser fluences are shown in (b) and (c), respectively. Solid lines are fits to the tr-XAS difference traces using the positive/negative Gaussian fit model (see Table 1).

resolved X-ray photoelectron experiments relying on the same X-ray/laser synchronization scheme.[39,43] Future experiments are planned to disentangle the characteristic rise time of the transient Cu_2O X-ray response and the instrument-limited time resolution. By analysing the tr-XAS spectra stemming from the multi-bunches after the camshaft, we find a mono-exponential decay with a characteristic time constant of 43 ± 5 ns as shown in Fig. 8.

The magnitude of the edge shift associated with the fast decaying response is analysed by applying the same fit procedure as for the quasi-static response.[35] Within this particular modelling, a strong dependence of the differential energy shift with pump–probe delay is found, decreasing from $\sim$2.2 eV at $\Delta t = 250$ ps down to $\sim$1.2 eV at $\Delta t = 180$ ns (see Table 1). However, we would like to emphasize that this analysis is associated with large uncertainties concerning the Gaussian peak line shapes. We therefore additionally report the energetic difference of the two extrema in the difference spectra, which do not depend on a specific fit model. This procedure yields spectral shifts of ~ -2 eV for all pump–probe delays, as noted in Table 2. Interestingly, this differential shift is comparable to the band gap energy of Cu_2O.[32–34] The corresponding model-free shift of the quasi-static

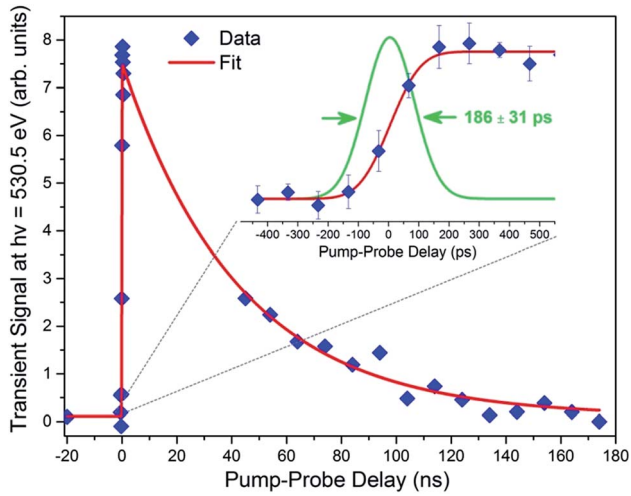

Fig. 8 Temporal evolution of the laser-induced transient change of the O1s XAS line shape probed at a photon energy of $h\nu = 530.5$ eV. The red solid line is a fit to a sum of a step function and a mono-exponential decay model (time constant 43 ± 5 ns) convoluted with a Gaussian. The inset highlights the sub-nanosecond rise time of the laser-induced X-ray response. Error bars denote standard errors of an average of 4 pump–probe delay scans.

response is 1.6 eV. The qualitative differences between the fast decaying and the quasi-static responses are readily apparent from the comparison of the differential tr-XAS curves in Fig. 6(b). While the fast decaying response corresponds to a larger shift in energy, its amplitude is about a factor of 9 smaller than that of the quasi-static response.

Discussion

Cuprous oxide is among the class of metal oxides under consideration for a variety of photo- and electrochemical applications.[29,30,32–35,46–50] Understanding the material's electronic and chemical properties under non-equilibrium conditions is important for the evaluation of its potential and fundamental limitations.

Table 1 Parameters extracted from a fit of the O1s tr-XAS difference spectra to a sum of positive- and negative-amplitude Gaussians (A = peak area; FWHM = full width at half maximum; E_{fit} = peak-to-peak separation of the two Gaussians)

Data	$A(+)$	$A(-)$	FWHM(+) [eV]	FWHM(−) [eV]	E_{fit} [eV]
Hillyard *et al.*[35]	0.19	0.28	0.99	2.15	1.14
Static diff. 10 mJ cm^{-2}	3.09	2.52	1.60	2.01	0.78
$\Delta t = 250$ ps@6 mJ cm^{-2}	0.16	0.10	1.40	2.07	2.17
$\Delta t = 250$ ps@10 mJ cm^{-2}	0.25	0.15	1.81	2.36	1.94
$\Delta t = 45$ ns@10 mJ cm^{-2}	0.11	0.16	1.37	2.94	1.65
$\Delta t = 180$ ns@10 mJ cm^{-2}	0.09	0.13	1.67	2.76	1.15

Table 2 Model-independent key parameters of the tr-XAS O1s difference spectra of Cu_2O: integrals over the positive (Int(+)) and negative (Int(−)) parts of the difference spectra and the energetic separation between the maximum and minimum Δmax/min

Data	Int(+)	Int(−)	Δmax/min [eV]
Hillyard *et al.*[35]	0.097	0.185	1.3
Static diff. 10 mJ cm^{-2}	1.471	0.910	1.6
$\Delta t = 250$ ps@6 mJ cm^{-2}	0.145	0.081	2.2
$\Delta t = 250$ ps@10 mJ cm^{-2}	0.197	0.104	2.2
$\Delta t = 45$ ns@10 mJ cm^{-2}	0.032	0.070	2.0
$\Delta t = 180$ ns@10 mJ cm^{-2}	0.035	0.064	1.9

The ground state electronic structure and the electronic excitation spectrum of Cu_2O have long been a matter of continued discussions.[32–35,40–42,50–55] Whereas the excitonic spectrum of Cu_2O is well understood and often serves as a textbook example for bound electron–hole excitations in condensed matter systems,[33,53] other fundamental properties such as the extent of the band gap and the relative orbital contributions to different portions of the VB and CB are subject to ongoing debate.[35,40,42,52,53,56–59] X-ray spectroscopy studies are particularly well suited to probe the density and character of occupied and unoccupied states, employing element specific transitions with well-defined selection rules.[40,57,59–61] An extension of this class of experiments to optical-pump/X-ray-probe studies, whereby inner-shell transitions are employed to monitor *transient* valence electronic configurations, may provide not only complementary information on the character of VB and CB states, but also their dynamic evolution under non-equilibrium conditions that are relevant for many envisioned applications of the material.[16,35,62–65]

The picosecond tr-XAS experiments described here reveal two types of laser-induced dynamic responses in the O1s XAS spectrum of Cu_2O. Excitation with 355 nm laser pulses at fluences of ~6–10 mJ cm^{-2} leads to both a fast (~ns) and a slowly ($\gg 8$ μs) decaying, reversible line shape change of the dominant XAS feature at $h\nu = 532$ eV. Without state-of-the-art theory support, it is challenging to provide details on the nature of the electronic configurations that induce the observed tr-XAS signals. Nevertheless, some qualitative results are readily apparent and may be discussed in the context of previous studies and general considerations concerning transient XAS experiments on condensed phase systems.

The slow response manifests itself in a quasi-static redshift of the absorption edge by approximately 1 eV. Interestingly, this value reproduces the results of Gaffney and co-workers who studied a 50 nm thick film of Cu_2O by tr-XAS in transmission geometry using 400 nm excitation at essentially the same pulse fluences as used in our experiment but at a laser repetition rate of only 1 kHz.[35] In their study, a ~1 eV redshift was the only observed response within the ±200 ps pump–probe delay range accessible in their experiment, and it was observed as a transient response, *i.e.*, it fully relaxed on the 1 ms timescale between laser pulses. Given the similarities between the observed shifts, we speculate that the quasi-static response observed in our experiment may be linked to the same underlying physics as the transient response detected by Hillyard *et al.*, and that

the different temporal evolution (quasi-static *vs.* transient) are caused by the significantly different laser repetition rates. Within this picture, the lifetime of the configurations leading to the ~1 eV O1s XAS shift would have to be on the order of 8 μs $\ll \Delta t \ll$ 1 ms. In fact, among direct-band gap semiconductors, Cu_2O is known to exhibit unusually long excitonic lifetimes due to dipole-forbidden recombination channels.[66,67] Previous studies reported charge carrier recombination timescales ranging from sub-nanosecond to milliseconds depending on the quality of the sample and its temperature.[67–69] It is, therefore, possible that the combination of high repetition rate laser excitation and long-lived excited electronic configurations leads to a build-up of electron–hole states that appear as a significant, quasi-static differential tr-XAS signal as shown in Fig. 6.

As noted by Hillyard *et al.*,[35] the observed XAS edge shift corresponds to only about half of the 2.2 eV optical band gap energy of Cu_2O.[32–34] At first glance this seems somewhat surprising. On the timescales accessible with the experiment, holes and photoexcited electrons are expected to have relaxed to the top of the VB and the bottom of the CB, respectively.[35,66] As holes in previously occupied VB states may lead to enhanced inner-shell absorption below the ground state XAS edge and the filling of usually unoccupied CB states with photoexcited electrons may suppress transitions in the XAS spectrum at higher energies, one may expect an effective redshift in the tr-XAS spectrum where the depletion and enhancement regions are separated by the band gap energy. While the direction of the observed shift conforms to this basic model, its magnitude clearly does not. We note that even more advanced multi-body models predict an X-ray edge shift after super-band gap excitation comparable to the band gap provided that only VB and CB states are involved in the photo-induced dynamics. The discrepancies between the experimental results and general expectations for tr-XAS spectra can, therefore, not readily be explained and we resort to a discussion of possible contributing factors.

One tempting explanation for an apparently reduced energy gap may be the involvement of mid-gap states. For example, impurity and/or defect induced trap states may be abundant in the pellet sample used in this study and could be located in the nominal band gap of single crystalline Cu_2O. Such states may also be associated with very long lifetimes, which would explain the observed saturation effect leading to the quasi-static response. Even then, however, the amplitude of the quasi-static photo-induced effect, which amounts to ~30% of the maximum static XAS signal, seems unusually large to be associated with mid-gap states. More information on the possible involvement of such states will be gained from a complementary optical characterization of the samples.

More generally, the simple model outlined above for expected photo-induced XAS edge shifts does not take the localized nature of inner-shell transitions and final state effects in core-excited configurations into account.[41,70,71] Previous time-resolved inner-shell absorption studies have demonstrated that, depending on the character of the involved valence configurations, transient XAS shifts in condensed phase systems are sometimes better described in a localized picture of atomic oxidation state changes rather than within a delocalized band model.[16,62,63] This trend is expected to be particularly pronounced for materials with strong ionic bonding character, such as transition metal oxides, where the valence orbitals are significantly localized.[53,63] Several studies have pointed out that, despite a nominally filled Cu3d shell, which dominates both the occupied and

unoccupied electronic states near the VB and CB edges, respectively, bonding in Cu_2O is not purely ionic but also exhibits notable contributions of hybridization and covalent bonding involving Cu3d, Cu4s, and O2p states.[40–42,57] X-ray transitions in this material may therefore bear signatures of both localized and delocalized valence orbital configurations and the correlation between optical excitations and corresponding changes in X-ray absorption is non-trivial, even without taking core-hole relaxation into account. We note, however, that a strong charge-transfer between Cu and O atomic sites is not expected for electron/hole configurations that have relaxed to the CB/VB edges. This is supported by the tr-XAS results of Hillyard *et al.* who find almost identical redshifts for the Cu2p and O1s edges and theoretical calculations that predict a mixed Cu3d/O2p orbital character near both the VB and the CB edges.[41,42,57]

Self-energy (also termed relaxation, screening, polarization, or reorganization) corrections in the core-excited states may further complicate a straightforward interpretation of the transient difference spectrum.[41,61,70,71] These corrections are the result of the response of all electrons in a system to the creation of a core-hole. The electron/core-hole interaction may lower the energy of the final state by several tens of eV compared to the first-order picture of non-interacting electrons (for atoms with $Z \leq 30$).[71] However, in view of the results presented here, the corrections would have to be *different* for excitations of O1s electrons into VB and CB vacancies in order to affect the magnitude of the observed transient XAS shift, which would imply different electron/core-hole interactions and, therefore, different orbital configurations at the VB and CB edges. In this case, however, one may also expect a difference in the cross sections for core-excitation into VB and CB vacancies, which would result in different magnitudes of the tr-XAS suppression and enhancement features. Interestingly, such an asymmetry is indeed observed (see Fig. 7(b and c)). Integration over the positive and negative slopes of the differential absorption spectra at 250 ps delay reveals that the transient signal enhancement exceeds the signal suppression by a factor of 1.9 and 2.0 for pump laser fluences of 6 mJ cm^{-2} and 10 mJ cm^{-2}, respectively. While the difference between these two numbers may not be significant, their absolute values indicate an enhanced X-ray absorption involving VB compared to CB vacancies. This finding would be consistent with a difference in electronic character of the occupied (VB) and unoccupied (CB) band edge states and, therefore, a difference in core-hole relaxation energies seems possible.

We note that Hillyard *et al.* found no definitive evidence for an asymmetry in their tr-XAS difference spectra and concluded that the contributions of Cu3d and O2p orbitals to the VB and CB edges must be very similar.[35] We are unable to provide a conclusive explanation for the differences in the observed asymmetries but we point out that the two studies were not performed under identical conditions. The sample for the transmission-based experiment was a 50 nm polycrystalline film of Cu_2O deposited on a silicon nitride membrane, whereas an $\sim$2 mm thick pellet of Cu_2O powder was used for the TFY based experiment reported here. Perhaps the most significant difference is an increase in the average laser exposure by about two orders of magnitude in the current experiment (127 kHz compared to 1 kHz), which may lead to saturation effects as indicated by the quasi-static response illustrated in Fig. 6. Future studies using thin films of Cu_2O, lower pulse repetition rates, and, potentially, lower peak fluences, will provide more information on the interplay between these parameters and the observed spectral X-ray responses.

Principally, structural effects (in addition to purely electronic dynamics) need to be taken into account. Reversible solid–liquid phase changes in germanium (Ge), *e.g.*, have previously been shown to produce tr-XAS changes on similar orders of magnitude as observed for the quasi-static Cu_2O response.[28] Inducing these changes, however, required more than an order of magnitude higher laser fluences ($\sim$120 mJ cm^{-2}) compared to the experiment presented here. Given the very similar melting points of Cu_2O and Ge, it is unlikely that the comparably small fluence of the current experiment could induce a similar phase change. The solid phase of Ge was completely restored within $\sim$200 ns after laser excitation, which is very small compared to the $\gg 8$ μs lifetime of the quasi-static response observed here.

For completeness, we mention that, in principle, a completely different effect could also cause a deviation of tr-XAS redshift from the optical band gap energy of Cu_2O. Based on first principles, self-consistent orthogonalized linear combination of atomic orbitals (OLCAO) calculations, Ching and co-workers predicted that the intrinsic band gap of Cu_2O is on the order of only 0.8 eV and that the difference between this value and the optically measured band gap of 2.2 eV is due to symmetry-forbidden transitions.[55] Given the similarity of this intrinsic band gap estimate with the spectral shifts observed in both tr-XAS studies on Cu_2O, it might be tempting to draw parallels between the theoretical and experimental results. However, the local density approximation (LDA) approach associated with OLCAO is known to underestimate band gap values by significant margins,[57,72] and neither current state-of-the-art methods that go beyond LDA[53,72] nor alternative experimental methods to measure the band gap[60] seem to reproduce the OLCAO result. We, therefore, conclude that the most likely reasons for the relatively small photo-induced tr-XAS shift compared to the optical band gap may be related to mid-gap states, core-hole relaxation effects and, potentially, the impact of localized valence electron configurations. Clearly, more high-level theory efforts are needed to provide a more conclusive explanation of this phenomenon.

Concerning the fast-decaying response, a closer inspection of the tr-XAS spectra reveals that the maximum relative changes in the absorption spectrum associated with this response are on the order of $\approx$4–12% ($\approx$18–56 mOD). These difference amplitudes are essentially the same for both laser pulse fluences of 6 mJ cm^{-2} and 10 mJ cm^{-2}. However, the absorption enhancement feature recorded with the higher fluence extends to lower photon energies by $\approx$0.5 eV while the depletion feature remains almost unchanged (Fig. 7(c)). Note that the peak of the enhancement feature appears at the same energy for both fluences (530.5 eV), only the shape changes. This effect already demonstrates a shortcoming of the simple Gaussian-based modelling of the tr-XAS features, which does not capture such subtle changes in a physically insightful way. Without further experimental and theoretical investigation, it is challenging to provide a better description and deeper interpretation of the observed spectral changes. Nevertheless, the observation provides additional evidence that, at least in the study presented here, transient depletion and enhancement features in the O1s tr-XAS spectrum of photoexcited Cu_2O are not mirror images of each other. This effect may be related to differences in electronic characters at the VB and CB edges, different relaxation dynamics of photogenerated holes and electrons, and/or the impact of saturation effects.

The $\sim$2 eV shift associated with the short-lived response has not been reported previously. Given the discussion on expected photo-induced XAS edge shifts

outlined above, it may be tempting to draw connections between the short-lived response and the 2.2 eV optical band gap of Cu_2O. While we cannot exclude a deeper physical connection, we emphasize that the saturation conditions that are evident by the quasi-static response may induce a non-trivial connection between the two observed effects. In the case of a saturated density of hole states at the VB edge, for example, additionally created holes may not be able to relax all the way to the VB edge within the expected picosecond time frame and, instead, lead to inner-shell transitions at lower energies on the nanosecond timescales observed in the experiment (Fig. 8(b)). The same concept would provide a qualitative explanation for the observed extension of the fast decaying response to lower energies upon increasing the pump fluence from 6 mJ cm^{-2} to 10 mJ cm^{-2} as illustrated in Fig. 7(c). Note that such an effect would not necessarily have to be symmetric for photo-induced holes and electrons (*i.e.*, tr-XAS enhancement and suppression) since the densities of states on both sides of the band gap are not identical.[60]

Conclusion and outlook

A newly developed tr-XAS experimental setup is presented that employs a fast time-tagging technique to simultaneously monitor transient changes in the XAS spectra of condensed phase samples across temporal scales from tens of picoseconds to hundreds of nanoseconds. A proof-of-concept experiment shows that photo-induced dynamics in a microporous Cu_2O powder sample after 355 nm excitation at fluences of 6–10 mJ cm^{-2} lead to two distinct responses in the O1s tr-XAS spectrum. A quasi-static shift of the ground state O1s XAS spectrum by $\sim$1 eV to lower energies indicates a lifetime of the corresponding transient configurations well beyond the 8 μs delay between laser pulses. An additional $\sim$2 eV redshift of the absorption edge appears within less than 200 ps and decays on a timescale of 43 $\pm$ 5 ns. While the amplitude of this effect is insensitive to a doubling of the laser fluence, the shape of the photo-induced enhanced absorption feature does vary and extends to lower energies for the higher fluence. Absorption enhancement and depletion features in both the fast decaying and the quasi-static response are not symmetric, with the photo-induced enhancement exceeding the depletion by a factor of $\sim$1.7–2.0.

All observed differential tr-XAS effects are tentatively assigned to transient, photo-induced electron–hole configurations governed by different lifetimes. The dominant quasi-static shift reproduces the transient shift observed by Gaffney and co-workers. We speculate that both observations are connected to similar underlying electronic dynamics and that the different appearances (quasi-static *vs.* transient) are linked to saturation effects in the present experiment due to the high laser repetition rate. The quasi-static shift cannot be explained within a picture that would suggest a shift of the X-ray absorption edge by the extent of the optical band gap energy of 2.2 eV. The qualitative difference between the expected and measured shifts may be connected to mid-gap states, core-hole relaxation effects, and/or the localized nature of core-hole transitions in combination with the at least partially localized nature of the Cu_2O valence orbitals. The XAS edge shift associated with the fast decaying response approximately matches the extent of the band gap. However, in view of the by far dominant quasi-static response, a direct connection might not be appropriate. A simple picture of

saturated hole/electron densities at the VB/CB edges associated with the quasi-static response provides a possible qualitative explanation for the difference between the two shifts and the observed trend of an increased redshift in the short-lived tr-XAS response with increasing laser fluence.

The observed asymmetries in all differential tr-XAS spectra may be an indication for different orbital mixtures in VB and CB states. However, we cannot exclude that excitation saturation effects may also play a role. A much larger body of experimental and, in particular, theoretical work is needed to give a conclusive interpretation of the observed effects. Nevertheless, the discussion demonstrates that the newly developed technique provides a wealth of information on the electronic structure and dynamics of photoactive metal oxide semiconductors from the viewpoint of well-defined atomic sites.

Extending the realm of time-domain X-ray spectroscopy techniques to non-replenishing condensed phase systems and, ultimately, operating photochemical devices holds great promise to capture transient electronic and chemical configurations that may be crucial for the overall function of a material or device but that are too short-lived to be tracked by steady-state spectroscopy techniques. X-ray absorption measurements using photon-in/photon-out techniques are already playing an important role in the static domain where *in situ* and *in operando* methods for the study of ongoing photochemical processes have significantly advanced over the past decade. Time-resolved XAS techniques – such as presented here – may provide a route toward monitoring ongoing chemical transformations with the atomic site specificity and chemical sensitivity provided by inner-shell transitions, in particular, when combined with state-of-the-art *in operando* X-ray spectroscopy components.

Acknowledgements

This work was supported by the U.S. Department of Energy, Office of Basic Energy Sciences, Chemical Sciences, Geosciences and Biosciences Division, through Contract No. DE-AC02-05CH11231. O. G. was supported by the Department of Energy Office of Science Early Career Research Program. S. N. acknowledges support by the Alexander von Humboldt foundation. We would like to thank Dr C. D. Pemmaraju for stimulating discussions and the staff of the Advanced Light Source for help and assistance. The Advanced Light Source is supported by the Director, Office of Science, Office of Basic Energy Sciences, of the U.S. Department of Energy under Contract No. DE-AC02-05CH11231.

References

1 O. Fuchs, F. Maier, L. Weinhardt, M. Weigand, M. Blum, M. Zharnikov, J. Denlinger, M. Grunze, C. Heske and E. Umbach, *Nucl. Instrum. Methods Phys. Res., Sect. A*, 2008, **585**, 172–177.

2 A. Braun, K. Sivula, D. K. Bora, J. Zhu, L. Zhang, M. Grätzel, J. Guo and E. C. Constable, *J. Phys. Chem. C*, 2012, **116**, 16870–16875.

3 N. Becknell, Y. Kang, C. Chen, J. Resasco, N. Kornienko, J. Guo, N. M. Markovic, G. A. Somorjai, V. R. Stamenkovic and P. Yang, *J. Am. Chem. Soc.*, 2015, **137**, 15817–15824.

4 S. Nemšák, A. Shavorskiy, O. Karslioglu, I. Zegkinoglou, A. Rattanachata, C. S. Conlon, A. Keqi, P. K. Greene, E. C. Burks, F. Salmassi, E. M. Gullikson, S.-H. Yang, K. Liu, H. Bluhm and C. S. Fadley, *Nat. Commun.*, 2014, **5**, 5441.
5 E. Gross, X.-Z. Shu, S. Alayoglu, H. A. Bechtel, M. C. Martin, F. D. Toste and G. A. Somorjai, *J. Am. Chem. Soc.*, 2014, **136**, 3624–3629.
6 D. N. Mueller, M. L. Machala, H. Bluhm and W. C. Chueh, *Nat. Commun.*, 2015, **6**, 6097.
7 E. J. Crumlin, Z. Liu, H. Bluhm, W. Yang, J. Guo and Z. Hussain, *J. Electron. Spectros. Relat. Phenom.*, 2015, **200**, 264–273.
8 H. Ali-Löytty, M. W. Louie, M. R. Singh, L. Li, H. G. Sanchez Casalongue, H. Ogasawara, E. J. Crumlin, Z. Liu, A. T. Bell, A. Nilsson and D. Friebel, *J. Phys. Chem. C*, 2016, **120**, 2247–2253.
9 A. H. Zewail, *J. Phys. Chem. A*, 2000, **104**, 5660–5694.
10 Z.-H. Loh and S. R. Leone, *J. Phys. Chem. Lett.*, 2013, **4**, 292–302.
11 A. R. Attar, A. Bhattacherjee and S. R. Leone, *J. Phys. Chem. Lett.*, 2015, **6**, 5072–5077.
12 H. Dachraoui, M. Michelswirth, P. Siffalovic, P. Bartz, C. Schäfer, B. Schnatwinkel, J. Mattay, W. Pfeiffer, M. Drescher and U. Heinzmann, *Phys. Rev. Lett.*, 2011, **106**, 107401.
13 C. Bressler and M. Chergui, *Annu. Rev. Phys. Chem.*, 2010, **61**, 263–282.
14 M. Saes, C. Bressler, R. Abela, D. Grolimund, S. Johnson, P. Heimann and M. Chergui, *Phys. Rev. Lett.*, 2003, **90**, 047403.
15 W. Gawelda, M. Johnson, F. M. F. de Groot, R. Abela, C. Bressler and M. Chergui, *J. Am. Chem. Soc.*, 2006, **128**, 5001–5009.
16 M. H. Rittmann-Frank, C. J. Milne, J. Rittmann, M. Reinhard, T. J. Penfold and M. Chergui, *Angew. Chem., Int. Ed.*, 2014, **53**, 5858–5862.
17 L. X. Chen, *Annu. Rev. Phys. Chem.*, 2005, **56**, 221–254.
18 B. E. Van Kuiken, N. Huse, H. Cho, M. L. Strader, M. S. Lynch, R. W. Schoenlein and M. Khalil, *J. Phys. Chem. Lett.*, 2012, **3**, 1695–1700.
19 N. Huse, H. Cho, K. Hong, L. Jamula, F. M. F. de Groot, T. K. Kim, J. K. McCusker and R. W. Schoenlein, *J. Phys. Chem. Lett.*, 2011, **2**, 880–884.
20 P. Wernet, K. Kunnus, I. Josefsson, I. Rajkovic, W. Quevedo, M. Beye, S. Schreck, S. Grubel, M. Scholz, D. Nordlund, W. Zhang, R. W. Hartsock, W. F. Schlotter, J. J. Turner, B. Kennedy, F. Hennies, F. M. F. de Groot, K. J. Gaffney, S. Techert, M. Odelius and A. Fohlisch, *Nature*, 2015, **520**, 78–81.
21 H. Öström, H. Öberg, H. Xin, J. LaRue, M. Beye, M. Dell'Angela, J. Gladh, M. L. Ng, J. A. Sellberg, S. Kaya, G. Mercurio, D. Nordlund, M. Hantschmann, F. Hieke, D. Kühn, W. F. Schlotter, G. L. Dakovski, J. J. Turner, M. P. Minitti, A. Mitra, S. P. Moeller, A. Föhlisch, M. Wolf, W. Wurth, M. Persson, J. K. Nørskov, F. Abild-Pedersen, H. Ogasawara, L. G. M. Pettersson and A. Nilsson, *Science*, 2015, **347**, 978–982.
22 M. Dell'Angela, T. Anniyev, M. Beye, R. Coffee, A. Föhlisch, J. Gladh, T. Katayama, S. Kaya, O. Krupin, J. LaRue, A. Møgelhøj, D. Nordlund, J. K. Nørskov, H. Öberg, H. Ogasawara, H. Öström, L. G. M. Pettersson, W. F. Schlotter, J. A. Sellberg, F. Sorgenfrei, J. J. Turner, M. Wolf, W. Wurth and A. Nilsson, *Science*, 2013, **339**, 1302–1305.
23 K. R. Siefermann, C. D. Pemmaraju, S. Neppl, A. Shavorskiy, A. A. Cordones, J. Vura-Weis, D. S. Slaughter, F. P. Sturm, F. Weise, H. Bluhm, M. L. Strader, H. Cho, M.-F. Lin, C. Bacellar, C. Khurmi, J. Guo, G. Coslovich,

J. S. Robinson, R. A. Kaindl, R. W. Schoenlein, A. Belkacem, D. M. Neumark, S. R. Leone, D. Nordlund, H. Ogasawara, O. Krupin, J. J. Turner, W. F. Schlotter, M. R. Holmes, M. Messerschmidt, M. P. Minitti, S. Gul, J. Z. Zhang, N. Huse, D. Prendergast and O. Gessner, *J. Phys. Chem. Lett.*, 2014, **5**, 2753–2759.

24 W. K. Zhang, R. Alonso-Mori, U. Bergmann, C. Bressler, M. Chollet, A. Galler, W. Gawelda, R. G. Hadt, R. W. Hartsock, T. Kroll, K. S. Kjaer, K. Kubicek, H. T. Lemke, H. Y. W. Liang, D. A. Meyer, M. M. Nielsen, C. Purser, J. S. Robinson, E. I. Solomon, Z. Sun, D. Sokaras, T. B. van Driel, G. Vanko, T. C. Weng, D. L. Zhu and K. J. Gaffney, *Nature*, 2014, **509**, 345.

25 S. E. Canton, K. S. Kjær, G. Vankó, T. B. van Driel, S.-i. Adachi, A. Bordage, C. Bressler, P. Chabera, M. Christensen, A. O. Dohn, A. Galler, W. Gawelda, D. Gosztola, K. Haldrup, T. Harlang, Y. Liu, K. B. Møller, Z. Németh, S. Nozawa, M. Pápai, T. Sato, T. Sato, K. Suarez-Alcantara, T. Togashi, K. Tono, J. Uhlig, D. A. Vithanage, K. Wärnmark, M. Yabashi, J. Zhang, V. Sundström and M. M. Nielsen, *Nat. Commun.*, 2015, **6**, 6359.

26 S. Neppl, Y.-S. Liu, C.-H. Wu, A. Shavorskiy, I. Zegkinoglou, T. Troy, D. S. Slaughter, M. Ahmed, A. S. Tremsin, J.-H. Guo, P.-A. Glans, M. Salmeron, H. Bluhm and O. Gessner, *Ultrafast Phenomena XIX*, 2014, vol. 162, pp. 325–327.

27 A. S. Tremsin, O. H. W. Siegmund, J. S. Hull, J. V. Vallerga, J. B. McPhate, J. Soderstrom, J. W. Chiou, J. Guo and Z. Hussain, *IEEE Nucl. Sci. Symp. Conf. Rec.*, 2006, **2**, 735–739.

28 L. Stebel, M. Malvestuto, V. Capogrosso, P. Sigalotti, B. Ressel, F. Bondino, E. Magnano, G. Cautero and F. Parmigiani, *Rev. Sci. Instrum.*, 2011, **82**, 123109.

29 M. Hara, T. Kondo, M. Komoda, S. Ikeda, J. N. Kondo, K. Domen, M. Hara, K. Shinohara and A. Tanaka, *Chem. Commun.*, 1998, 357–358, DOI: 10.1039/A707440I.

30 V. S. K. Yadav and M. K. Purkait, *Energy Fuels*, 2015, **29**, 6670–6677.

31 J. Y. Xiang, X. L. Wang, X. H. Xia, L. Zhang, Y. Zhou, S. J. Shi and J. P. Tu, *Electrochim. Acta*, 2010, **55**, 4921–4925.

32 M. A. Rafea and N. Roushdy, *J. Phys. D: Appl. Phys.*, 2009, **42**, 015413.

33 P. W. Baumeister, *Phys. Rev.*, 1961, **121**, 359–362.

34 S. Nikitine, J. B. Grun and M. Sieskind, *J. Phys. Chem. Solids*, 1961, **17**, 292–300.

35 P. W. Hillyard, S. V. N. T. Kuchibhatla, T. E. Glover, M. P. Hertlein, N. Huse, P. Nachimuthu, L. V. Saraf, S. Thevuthasan and K. J. Gaffney, *Phys. Rev. B: Condens. Matter Mater. Phys.*, 2009, **80**, 125210.

36 M. Saes, F. van Mourik, W. Gawelda, M. Kaiser, M. Chergui, C. Bressler, D. Grolimund, R. Abela, T. E. Glover, P. A. Heimann, R. W. Schoenlein, S. L. Johnson, A. M. Lindenberg and R. W. Falcone, *Rev. Sci. Instrum.*, 2004, **75**, 24–30.

37 F. A. Lima, C. J. Milne, D. C. V. Amarasinghe, M. H. Rittmann-Frank, R. M. v. d. Veen, M. Reinhard, V.-T. Pham, S. Karlsson, S. L. Johnson, D. Grolimund, C. Borca, T. Huthwelker, M. Janousch, F. van Mourik, R. Abela and M. Chergui, *Rev. Sci. Instrum.*, 2011, **82**, 063111.

38 A. M. March, A. Stickrath, G. Doumy, E. P. Kanter, B. Krässig, S. H. Southworth, K. Attenkofer, C. A. Kurtz, L. X. Chen and L. Young, *Rev. Sci. Instrum.*, 2011, **82**, 073110.

39 S. Neppl, A. Shavorskiy, I. Zegkinoglou, M. Fraund, D. S. Slaughter, T. Troy, M. P. Ziemkiewicz, M. Ahmed, S. Gul, B. Rude, J. Z. Zhang, A. S. Tremsin, P.-A. Glans, Y.-S. Liu, C. H. Wu, J. Guo, M. Salmeron, H. Bluhm and O. Gessner, *Faraday Discuss.*, 2014, **171**, 219–241.
40 P. Jiang, D. Prendergast, F. Borondics, S. Porsgaard, L. Giovanetti, E. Pach, J. Newberg, H. Bluhm, F. Besenbacher and M. Salmeron, *J. Chem. Phys.*, 2013, **138**, 024704.
41 M. Grioni, J. F. van Acker, M. T. Czyžyk and J. C. Fuggle, *Phys. Rev. B: Condens. Matter Mater. Phys.*, 1992, **45**, 3309–3318.
42 P. Marksteiner, P. Blaha and K. Schwarz, *Z. Phys. B: Condens. Matter*, 1986, **64**, 119–127.
43 S. Neppl and O. Gessner, *J. Electron Spectrosc. Relat. Phenom.*, 2015, **200**, 64–77.
44 R. Nakajima, J. Stöhr and Y. U. Idzerda, *Phys. Rev. B: Condens. Matter*, 1999, **59**, 6421–6429.
45 F. M. F. de Groot, M. Grioni, J. C. Fuggle, J. Ghijsen, G. A. Sawatzky and H. Petersen, *Phys. Rev. B: Condens. Matter Mater. Phys.*, 1989, **40**, 5715–5723.
46 B. K. Meyer, A. Polity, D. Reppin, M. Becker, P. Hering, P. J. Klar, T. Sander, C. Reindl, J. Benz, M. Eickhoff, C. Heiliger, M. Heinemann, J. Bläsing, A. Krost, S. Shokovets, C. Müller and C. Ronning, *Phys. Status Solidi B*, 2012, **249**, 1487–1509.
47 A. S. Zoolfakar, R. A. Rani, A. J. Morfa, A. P. O'Mullane and K. Kalantar-zadeh, *J. Mater. Chem. C*, 2014, **2**, 5247–5270.
48 P. E. de Jongh, D. Vanmaekelbergh and J. J. Kelly, *J. Electrochem. Soc.*, 2000, **147**, 486–489.
49 S. Somasundaram, C. Raman Nair Chenthamarakshan, N. R. de Tacconi and K. Rajeshwar, *Int. J. Hydrogen Energy*, 2007, **32**, 4661–4669.
50 A. Paracchino, J. C. Brauer, J.-E. Moser, E. Thimsen and M. Graetzel, *J. Phys. Chem. C*, 2012, **116**, 7341–7350.
51 S. Brahms, S. Nikitine and J. P. Dahl, *Phys. Lett.*, 1966, **22**, 31–33.
52 A. Filippetti and V. Fiorentini, *Phys. Rev. B: Condens.Matter Mater. Phys.*, 2005, **72**, 035128.
53 F. Bruneval, N. Vast, L. Reining, M. Izquierdo, F. Sirotti and N. Barrett, *Phys. Rev. Lett.*, 2006, **97**, 267601.
54 M. Nolan and S. D. Elliott, *Phys. Chem. Chem. Phys.*, 2006, **8**, 5350–5358.
55 W. Y. Ching, Y.-N. Xu and K. W. Wong, *Phys. Rev. B: Condens. Matter Mater. Phys.*, 1989, **40**, 7684–7695.
56 A. Önsten, M. Månsson, T. Claesson, T. Muro, T. Matsushita, T. Nakamura, T. Kinoshita, U. O. Karlsson and O. Tjernberg, *Phys. Rev. B: Condens. Matter Mater. Phys.*, 2007, **76**, 115127.
57 J. P. Hu, D. J. Payne, R. G. Egdell, P. A. Glans, T. Learmonth, K. E. Smith, J. Guo and N. M. Harrison, *Phys. Rev. B: Condens. Matter Mater. Phys.*, 2008, **77**, 155115.
58 M. M. Islam, B. Diawara, V. Maurice and P. Marcus, *J. Mol. Struct.*, 2009, **903**, 41–48.
59 Y.-J. Kim, J. P. Hill, H. Yamaguchi, T. Gog and D. Casa, *Phys. Rev. B: Condens. Matter Mater. Phys.*, 2010, **81**, 195202.
60 J. Ghijsen, L. H. Tjeng, J. van Elp, H. Eskes, J. Westerink, G. A. Sawatzky and M. T. Czyzyk, *Phys. Rev. B: Condens. Matter Mater. Phys.*, 1988, **38**, 11322–11330.
61 L. G. Parratt, *Rev. Mod. Phys.*, 1959, **31**, 616–645.

62 J. Vura-Weis, C.-M. Jiang, C. Liu, H. Gao, J. M. Lucas, F. M. F. de Groot, P. Yang, A. P. Alivisatos and S. R. Leone, *J. Phys. Chem. Lett.*, 2013, **4**, 3667–3671.
63 C.-M. Jiang, L. R. Baker, J. M. Lucas, J. Vura-Weis, A. P. Alivisatos and S. R. Leone, *J. Phys. Chem. C*, 2014, **118**, 22774–22784.
64 A. Cavalleri, M. Rini, H. H. W. Chong, S. Fourmaux, T. E. Glover, P. A. Heimann, J. C. Kieffer and R. W. Schoenlein, *Phys. Rev. Lett.*, 2005, **95**, 067405.
65 S. L. Johnson, P. A. Heimann, A. G. MacPhee, A. M. Lindenberg, O. R. Monteiro, Z. Chang, R. W. Lee and R. W. Falcone, *Phys. Rev. Lett.*, 2005, **94**, 057407.
66 D. W. Snoke, D. Braun and M. Cardona, *Phys. Rev. B: Condens. Matter Mater. Phys.*, 1991, **44**, 2991–3000.
67 A. Mysyrowicz, D. Hulin and A. Antonetti, *Phys. Rev. Lett.*, 1979, **43**, 1123.
68 R. Habiger and A. Compaan, *Solid State Commun.*, 1976, **18**, 1531–1534.
69 A. Jolk, M. Jörger and C. Klingshirn, *Phys. Rev. B: Condens. Matter Mater. Phys.*, 2002, **65**, 245209.
70 J. Stöhr, *NEXAFS spectroscopy*, Springer Science & Business Media, 2013.
71 F. Bechstedt, *Phys. Status Solidi B*, 1982, **112**, 9–49.
72 M. van Schilfgaarde, T. Kotani and S. Faleev, *Phys. Rev. Lett.*, 2006, **96**, 226402.

